Journal of Saudi Chemical Society (2015) **19**, 505–510

King Saud University

Journal of Saudi Chemical Society

www.ksu.edu.sa
www.sciencedirect.com

ORIGINAL ARTICLE

Preparation of nanosized yttrium doped CeO_2 catalyst used for photocatalytic application

A. Akbari-Fakhrabadi [a,*], R. Saravanan [b,*], M. Jamshidijam [c,d], R.V. Mangalaraja [c], M.A. Gracia [e]

[a] *Advanced Materials Laboratory, Department of Mechanical Engineering, University of Chile, Beauchef 851, Santiago, Chile*
[b] *Department of Chemical Engineering and Biotechnology, University of Chile, Beauchef 850, Santiago, Chile*
[c] *Advanced Ceramics and Nanotechnology Laboratory, Department of Materials Engineering, University of Concepcion, Concepcion, Chile*
[d] *Department of Materials Engineering, Islamic Azad University, Sirjan Branch, Sirjan, Iran*
[e] *Laboratorio de Nanociencias y Nanotecnología (FCFM), Universidad Autónoma de Nuevo León, Monterrey, Nuevo León, México*

Received 1 March 2015; revised 12 June 2015; accepted 15 June 2015
Available online 25 June 2015

KEYWORDS

Combustion synthesis;
Nanopowders;
Yttrium doped CeO_2;
Photocatalytic activity;
Rhodamine B

Abstract In the present work, the pure CeO_2 and yttrium doped CeO_2 nanopowders were synthesized by the nitrate-fuel self-sustaining combustion method and calcined at 700 °C for 2 h. X-ray diffraction (XRD) and high resolution electron transmission microscopy (HRTEM) results demonstrated a cubic fluorite with high purity and the crystallite sizes less than 20 nm calculated from Scherrer's formula. The BET specific surface area of yttrium doped CeO_2 samples showed high values than those of pure CeO_2. The photocatalytic activity of yttrium doped CeO_2 showed high degradation of Rhodamine B solution under visible light illumination.

1. Introduction

Water is essential for every living organism despite the fact that the quality and quantity of fresh water on earth is incomplete in accomplishing human needs. In the past years, the developing countries have met the dangerous effects on the environment due to the failure of pure water supply. Water contamination has led to major health risks which grow at a faster rate every year. According to a report given by the World Health Organisation (WHO), about 2.2 million people die due to water related problems every year, of these 90% are children [1]. Thus, water pollution creates major environmental issues around the globe. Nowadays, water gets polluted due to several reasons in the atmosphere such as population growth, releasing of effluents from industries and agricultural activities. In spite of so many factors that affect the quality of water, contaminants coming from the textile industries are one of the major causes for water pollution. In these industries, azodyes such as acid red 88 and methyl orange are used for dying purposes. These azodyes were found to have great

* Corresponding authors.
E-mail addresses: aliakbarif@ing.uchile.cl (A. Akbari-Fakhrabadi), saravanan3.raj@gmail.com (R. Saravanan).
Peer review under responsibility of King Saud University.

Production and hosting by Elsevier

http://dx.doi.org/10.1016/j.jscs.2015.06.003

hazardous effects on human health and environment [2–4]. One of the best ways to reduce the contamination of water is by photocatalytic treatment [2].

In the recent years, semiconductor based photocatalysts are attractive and significantly degrade the textile effluents. The large band gap semiconductors like titanium dioxide, zinc oxide, tin oxide are mostly used as photocatalytic materials due to their versatile properties such as thermal and chemical stability, low cost and eco-friendly [5–8]. Apart from these materials, cerium oxide (CeO_2) is one of the large bandgap semiconducting materials having lot of advantages and broad applications [9]. However, the CeO_2 is restricted to degrade pollution under visible light. The natural sunlight consists of ~45% visible region. Therefore, many researchers have focused in the field of photocatalyst that aims to increase the degradation efficiency in the visible light. Many efforts have been explored to extend the absorption wavelength of CeO_2 into the visible region by using metal doping, semiconductor coupling and so on [10–11]. Doping is a simple way to reduce the bandgap and led to extended photocatalytic activity from UV to visible light. Doping metal ion into cerium oxide effectively prevents the electron hole recombination and led to achieve photocatalytic activity under visible light.

In this present study, nanosized CeO_2 and yttrium doped CeO_2 were prepared by the combustion method as a simple and economical method. The structure and size of the prepared catalyst were analyzed by XRD and HR-TEM analysis. The surface area of the prepared material was examined by BET measurement. The optical bandgap of the catalysts was calculated using UV–Vis reflectance spectrometer measurements. Finally, the prepared catalysts were used to degrade Rhodamine B solution under visible light illumination and their results are discussed in detail.

2. Materials and methods

For the preparation of pure CeO_2 and yttrium doped CeO_2 nanopowders; all the required chemicals were purchased from Sigma–Aldrich and all the aqueous solutions were prepared using double distilled water.

The pure CeO_2 and yttrium doped CeO_2 nanopowders were synthesized by the nitrate-fuel self-sustaining combustion method. As the precursor reagents, the molecular proportions of the corresponding cerium and yttrium-nitrate hexahydrates were dissolved in 100 ml of double-distilled water to form a mixed homogeneous solution. Then, the required amount of citric acid, calculated from the basic principle of propellant chemistry [12], was added as an organic fuel. The equivalence ratio, i.e. the ratio of the oxidizing valency to the fuel was maintained at unity (O/F = 1) and the valency of nitrogen was not considered due to its conversion to molecular nitrogen (N_2) during combustion. After making a clear homogeneous precursor solution, the reaction mixture was transferred into an alumina crucible and inserted inside a preheated furnace at a temperature of 500 °C. Once the reaction mixture reached the point of spontaneous combustion, it started burning vigorously. As a result of the chemical reaction, porous solid foam was obtained within a few minutes. The as-combusted foams were collected and converted to powders by gentle grinding, and then calcined at 700 °C for 2 h to obtain full crystalline nanopowders [13,14].

2.1. Characterization details

Crystalline nature and phase purity were examined using the powder X-ray diffraction (XRD) technique (X'Pert Pro, Philips X-ray diffractometer) with Cu K_α radiation. The crystallite sizes were determined using Scherrer's equation [15]. The surface area of the prepared powders was obtained by the Br unauer–Emmett–Teller (BET) method [16]. Microstructures of the powders were analyzed by high resolution transmission electron microscopy (HR-TEM, FEI TITAN G2 80-300) operated at 300 kV. Compositional analysis was performed by scanning transmission electron microscopy (STEM) and energy dispersive X-ray spectroscopy (EDS) linked with TEM. The optical reflectance spectrum and the photocatalytic activity of the irradiated samples were measured by a UV–Visible spectrophotometer (Perkin Elmer Lambda 11).

3. Results and discussion

As demonstrated in Fig. 1, the X-ray diffraction patterns of the pure CeO_2 and yttrium doped CeO_2 powders show a single phase with cubic fluorite crystal structure, Fm3m space group [17,18], which shows full incorporation of yttrium dopant into the ceria lattice and forming a solid solution of the Y_2O_3–CeO_2 system [19,20]. Comparing the XRD pattern of pure CeO_2, the yttrium doped CeO_2 nanopowders revealed that the decrease in peak intensity and FWHM shows the minimum crystallite size [21].

Calculations based on the (1 1 1) diffraction peak's broadening in the XRD patterns represent that the crystallite sizes (D_{XRD}) of pure CeO_2 and yttrium doped CeO_2 nanopowders are 19.5 and 17 nm respectively, which were defined by using Scherrer's formula [15].

$$D_{XRD} = \frac{0.9\lambda}{B_{hkl}\cos\theta_{hkl}}$$

where B_{hkl} is the full width at half maximum (FWHM) excluding the instrumental broadening.

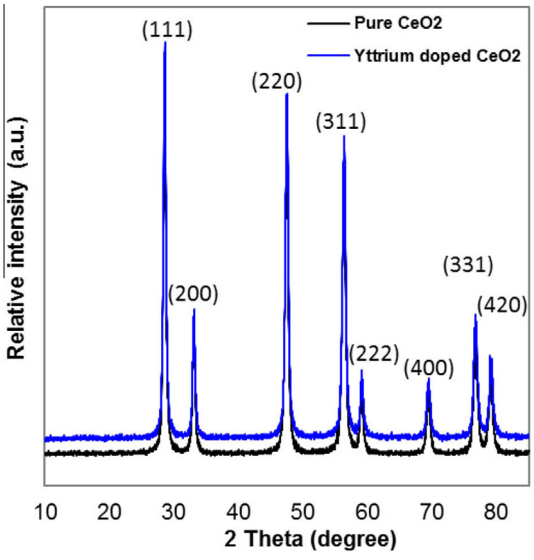

Figure 1 X-ray diffraction pattern of synthesized pure CeO_2 and yttrium doped CeO_2 nanopowders.

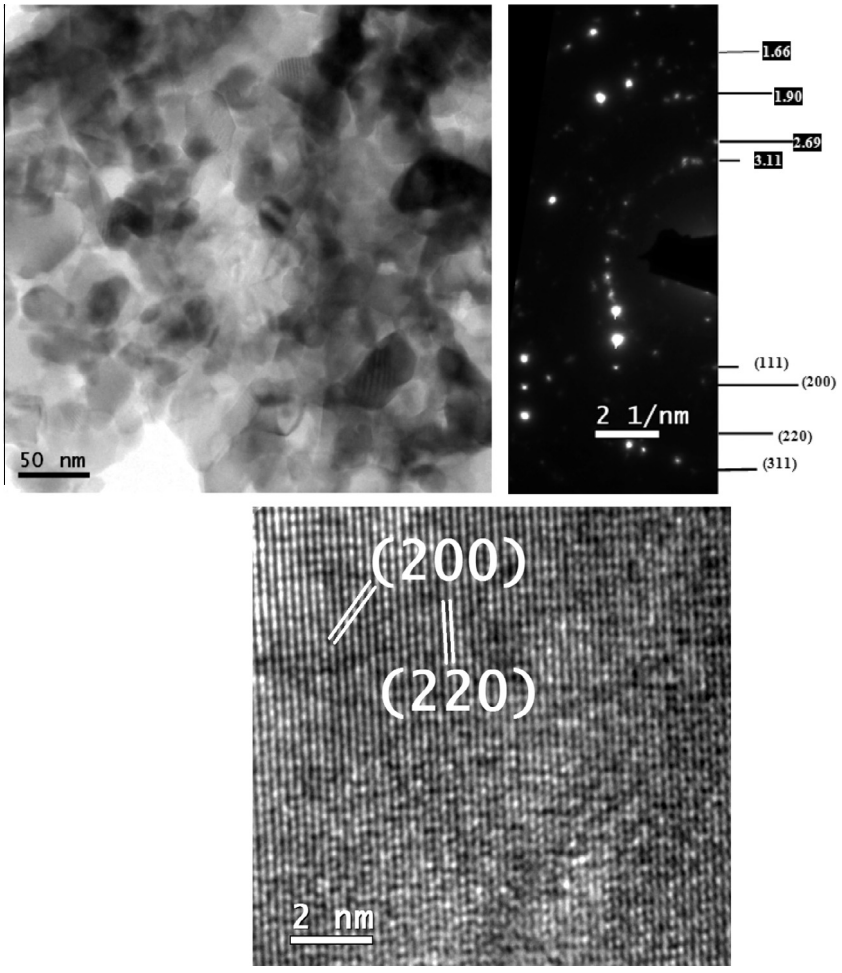

Figure 2 HRTEM images and diffraction pattern of pure CeO_2 nanopowders.

As shown in Table 1, primary particle size (D_{BET}) was calculated from the Brunauer–Emmett–Teller (BET) data according to the following relationship:

$$D_{BET} = \frac{6000}{\rho_{th} \cdot S_{BET}}$$

where S_{BET} (m^2/g) is the specific surface area with approximation of having closed spherical shape, smooth surface and uniform sized particles [22–24]. D_{BET} of the calcined pure ceria and yttrium doped ceria nanopowders are 30 and 23 nm, respectively. The decrease in size increases the surface area, which was confirmed from BET observation and the values are listed in Table 1.

The microstructures of pure CeO_2 and yttrium doped CeO_2 were characterized by HRTEM at low and high magnifications. Fig. 2 shows HRTEM images and the recorded selected area electron diffraction patterns (SAEDs) of pure CeO_2 nanopowders. As demonstrated in this pattern, the cubic fluorite structure could be indexed for this nanopowder, which confirms the XRD results. Micrographs show nanoparticles with size about 50 nm and clear internal crystal lattice structures. As shown in Fig. 3, HRTEM micrographs of yttrium doped CeO_2 also demonstrate the presence of clear internal crystal cubic fluorite structure and particle size in the range of 10–30 nm, which is smaller than those of pure CeO_2.

Table 1 Lattice parameter (a), crystallite size (D_{XRD}), specific surface area (S_{BET}) and primary particle size (D_{BET}) of pure CeO_2 and yttrium doped CeO_2.

Samples	a (nm)	D_{XRD} (nm)	D_{BET} (nm)	S_{BET} (m^2/g)
CeO_2	5.4123	17	30	36
Yttrium doped CeO_2	5.4057	19.5	23	52

The band gap values of the synthesized pure CeO_2 and yttrium doped CeO_2 nanomaterials were estimated from UV–Vis reflectance spectroscopy. Fig. 4 shows bandgap values of the prepared materials were determined by Kubelka–Munk function [10]. The bandgap (Eb_g) value of pure CeO_2 is around 3.31 eV and yttrium doped CeO_2 is 2.96 eV where the corresponding wavelength exists in the visible region. Hence, photocatalytic process mainly depends upon the wavelength of light which enhances the photocatalytic activity. The result of the reflectance spectra indicates that the visible light is an excellent source for the photocatalytic activity of yttrium doped CeO_2.

3.1. Photocatalytic degradation

The photocatalytic procedure was followed by previous literatures [11,25–27]. The prepared pure and yttrium doped CeO_2

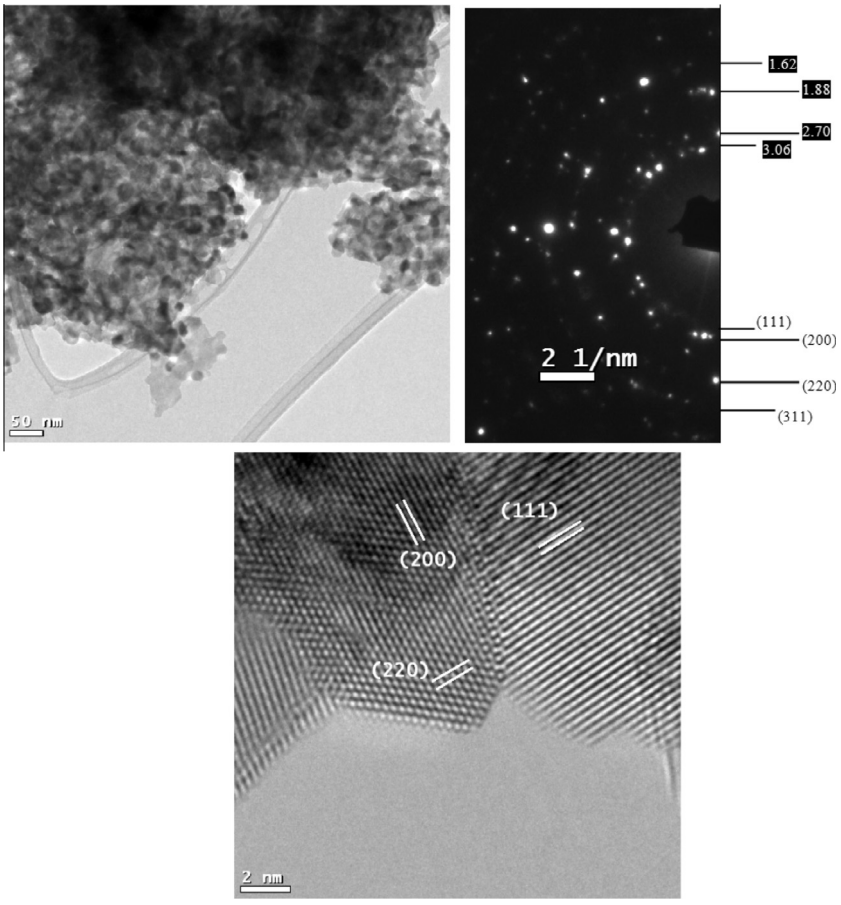

Figure 3 HRTEM images and diffraction pattern of yttrium doped CeO_2 nanopowders.

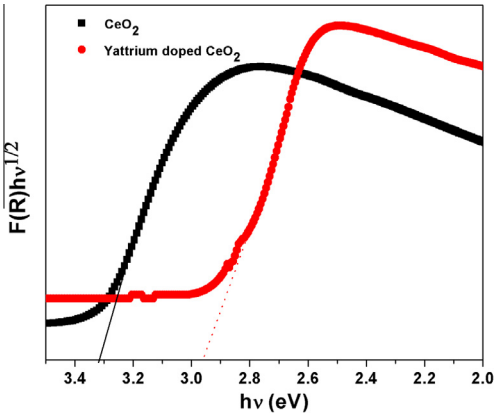

Figure 4 Determination of bandgap values of the prepared samples using K-M function.

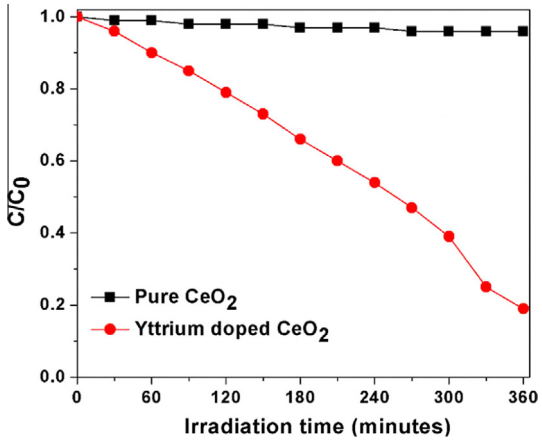

Figure 5 Time course degradation curve for 10 mg of prepared catalyst.

nanocatalysts were used to degrade aqueous Rhodamine B solution under visible light irradiation. Initially, the reaction suspensions were prepared by mixing the required amount of catalyst into 100 ml of aqueous rhodamine B (100 mg) solution in a 250 ml beaker. The source of visible light is a projection lamp (halogen lamp, Philips 7748XHP 250W G6.35 24V 1CT, ~532 nm) in a photoreactor. The reaction suspension was irradiated by regular intervals of time and these irradiated samples were collected (5 ml), centrifuged and filtered. Further, the absorption spectrum of irradiated aqueous Rhodamine B solutions was examined by UV–Visible spectrophotometer.

Fig. 5 represents the time course degradation curve (Rhodamine B) for pure and yttrium doped CeO_2 nanomaterials. It was observed that there is no degradation with the use of synthesized pure CeO_2 catalyst due to its large band gap [11]. During visible light irradiation, the wavelength of light is

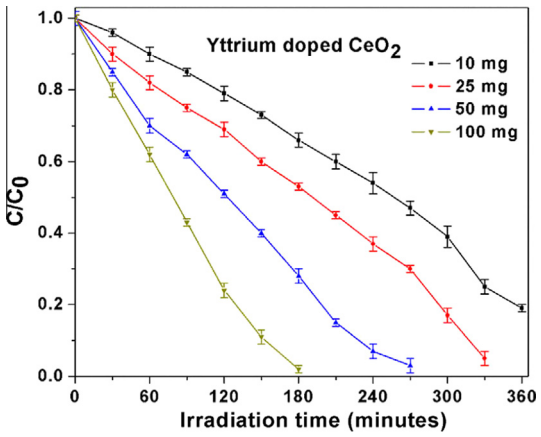

Figure 6 Time course degradation curve for different concentrations of yttrium doped CeO_2 catalyst.

insufficient for pure CeO_2 catalyst to make a pair electron and holes [11]. On the other hand, the yttrium doped CeO_2 effectively degrades the Rhodamine B solution under visible light for 6 h because of the lower bandgap value which lies in the visible region and this was confirmed from UV–Visible reflectance spectrum. Also, visible light irradiated on the surface of yttrium doped CeO_2 catalyst effectively produces electrons and holes by reduction and oxidation process during the photocatalytic reaction due to higher surface area of yttrium doped CeO_2 compared with pure CeO_2 [28–29]. These electrons and holes react with aqueous Rhodamine B solution and thus produce OH radicals which are capable for the effective degradation of Rhodamine B solution.

Furthermore, different concentrations of yttrium doped CeO_2 (10 mg, 25 mg, 50 mg and 100 mg) catalysts were carried out to degrade the Rhodamine B solution. The photocatalytic reaction was repeated three times under the same condition. As the time course degradation curve represented in Fig. 6 clearly shows, with increasing amount of catalyst, the degradation efficiency also increases. The error bar diagram indicates that the variation of degradation is very low when the photocatalytic activity was repeated three times. Therefore, the prepared yttrium doped CeO_2 catalyst sample having long time stability and recycling ability is favorable for environmental applications.

4. Conclusion

The pure CeO_2 and yttrium doped CeO_2 nanopowders were successfully synthesized by cost effective and easy combustion method. The characterization results confirm the doping of yttrium into CeO_2 does not change the cubic fluorite structure. The yttrium doped CeO_2 exhibits high surface area and lower bandgap compared with pure CeO_2. The photocatalytic activity of yttrium doped CeO_2 shows high degradation of Rhodamine B solution under visible light due to its size, high surface area and lower bandgap.

Acknowledgement

The authors acknowledge FONDECYT, Government of Chile, Santiago (Project Nos. 3140180 and 1130916) for the financial support to carry out this project.

References

[1] The World Health Report 2013: Research for Universal Health Coverage, World Health Organization, 2013.
[2] A. Fujishima, K. Honda, Electrochemical photolysis of water at a semiconductor electrode, Nature 238 (1972) 37–38.
[3] Y. Jiang, Y. Sun, H. Liu, F. Zhu, H. Yin, Solar photocatalytic decolorization of C.I. Basic Blue 41 in an aqueous suspension of TiO2–ZnO, Dyes Pigm. 78 (2008) 77–83.
[4] B.J. Sanghavi, O.S. Wolfbeis, T. Hirsch, N.S. Swami, Nanomaterial-based electrochemical sensing of neurological drugs and neurotransmitters, Microchim. Acta 182 (2015) 1–41.
[5] M.M. Khan, S.A. Ansari, D. Pradhan, M.O. Ansari, D.H. Han, J. Lee, M.H. Cho, Band gap engineered TiO_2 nanoparticles for visible light induced photoelectrochemical and photocatalytic studies, J. Mater. Chem. A 2 (2014) 637–644.
[6] R. Saravanan, E. Thirumal, V.K. Gupta, V. Narayanan, A. Stephen, The photocatalytic activity of ZnO prepared by simple thermal decomposition method at various temperatures, J. Mol. Liq. 177 (2013) 394–401.
[7] S. Kalathil, M.M. Khan, S.A. Ansari, J. Lee, M.H. Cho, Band gap narrowing of titanium dioxide (TiO2) nanocrystals by electrochemically active biofilms and their visible light activity, Nanoscale 5 (2013) 6323–6326.
[8] R. Saravanan, V.K. Gupta, V. Narayanan, A. Stephen, Comparative study on photocatalytic activity of ZnO prepared by different methods, J. Mol. Liq. 181 (2013) 133–141.
[9] M.M. Khan, S.A. Ansari, D. Pradhan, D.H. Han, J. Lee, M.H. Cho, Defect-induced band Gap narrowed CeO_2 nanostructures for visible light activities, Ind. Eng. Chem. Res. 53 (2014) 9754–9763.
[10] M.M. Khan, S.A. Ansari, J.H. Lee, M.O. Ansari, J. Lee, M.H. Cho, Electrochemically active biofilm assisted synthesis of Ag@CeO_2 nanocomposites for antimicrobial activity, photocatalysis and photoelectrodes, J. Colloid Interface Sci. 431 (2014) 255–263.
[11] R. Saravanan, S. Joicy, V.K. Gupta, V. Narayanan, A. Stephen, Visible light induced degradation of methylene blue using CeO_2/V_2O_5 and CeO_2/CuO catalysts, Mater. Sci. Eng. C 33 (2013) 4725–4731.
[12] S. Ekambaram, K.C. Patil, Combustion synthesis of yttria, J. Mater. Chem. 6 (1995) 905–908.
[13] A. Akbari-Fakhrabadi, R.V. Mangalaraja, M.A. Gracia Pinilla, M. Jamshidijam, Structural studies on the gadolinium doped nanoceria prepared by combustion synthesis, Mater. Lett. 125 (2014) 19–24.
[14] T.S. Zhang, J. Ma, L.B. Kong, P. King, J.A. Kilner, Preparation and mechanical properties of dense $Ce_{0.8}Gd_{0.2}O_{2-\delta}$ ceramics, Solid State Ionics 167 (2004) 191–196.
[15] B.D. Cullity, Elements of X-ray Diffraction, 2nd ed., Addison-Wesley, MA, 1978.
[16] S. Brunauer, P.H. Emmett, E. Teller, Adsorption of gases in multimolecular layers, J. Am. Chem. Soc. 60 (1938) 309–319.
[17] M. Kahlaoui, S. Chefi, A. Inoubli, A. Madani, Ch. Chefi, Synthesis and electrical properties of co-doping with La^{3+}, Nd^{3+}, Y^{3+}, and Eu^{3+} citrate–nitrate prepared samarium-doped ceria ceramics, Ceram. Int. 39 (2013) 3873–3879.
[18] T. Hisashige, Y. Yamamura, T. Tsuji, Thermal expansion and debye temperature of rare earth-doped ceria, J. Alloys Compd. 408–412 (2006) 1153–1156.
[19] B. Matovic, Z. Dohcevic-Mitrovic, M. Radovic, Z. Brankovic, G. Brankovic, S. Boskovic, Z.V. Popovic, Synthesis and characterization of ceria based nanometric powders, J. Power Sources 193 (2009) 146–149.
[20] S. Sameshima, H. Ono, K. Higashi, K. Sonoda, Y. Hirata, Microstructure of rare earth-doped ceria prepared by oxalate co-precipitation method, J. Ceram. Soc. Jpn. 108 (11) (2000) 985–988.

[21] V.D. Mote, Y. Purushotham, B.N. Dole, Williamson–Hall analysis in estimation of lattice strain in nanometer-sized ZnO particles, J. Theor. Appl. Phys. 6 (1) (2012) 1–8.
[22] Kumar, S. Babu, A.S. Karakoti, A. Schulte, S. Seal, Luminescence properties of europium-doped cerium oxide nanoparticles: role of vacancy and oxidation states, Langmuir 25 (18) (2009) 10998–11007.
[23] Y.P. Fu, S.H. Chen, Preparation and characterization of neodymium-doped ceria electrolyte materials for solid oxide fuel cells, Ceram. Int. 36 (2010) 483–490.
[24] Ch. Veranitisagul, A. Kaewvilai, W. Wattanathana, N. Koonsaeng, E. Traversa, A. Laobuthee, Electrolyte materials for solid oxide fuel cells derived from metal complexes: gadolinia-doped ceria, Ceram. Int. 38 (2012) 2403–2409.
[25] R. Saravanan, N. Karthikeyan, V.K. Gupta, P. Thangadurai, V. Narayanan, A. Stephen, ZnO/Ag nanocomposite: an efficient catalyst for degradation studies of textile effluents under visible light, Mater. Sci. Eng., C 33 (2013) 2235–2244.
[26] R. Saravanan, H. Shankar, T. Prakash, V. Narayanan, A. Stephen, ZnO/CdO composite nanorods for photocatalytic degradation of methylene blue under visible light, Mater. Chem. Phys. 125 (2011) 277–280.
[27] R. Saravanan, V.K. Gupta, V. Narayanan, A. Stephen, Visible light degradation of textile effluent using novel catalyst ZnO/γ-Mn_2O_3, J. Taiwan Inst. Chem. Eng. 45 (2014) 1910–1917.
[28] S.A. Ansari, M.M. Khan, M.O. Ansari, J. Lee, M.H. Cho, Visible light-driven photocatalytic and photoelectrochemical studies of Ag–SnO_2 nanocomposites synthesized using an electrochemically active biofilm, RSC Adv. 4 (2014) 26013–26021.
[29] S.A. Ansari, M.M. Khan, M.O. Ansari, M.H. Cho, Gold nanoparticles-sensitized wide and narrow band gap TiO_2 for visible light applications: a comparative study, New J. Chem. 39 (2015) 4708–4715.